optica

Femtosecond fiber lasers reach the mid-infrared

Simon Duval,* Martin Bernier, Vincent Fortin, Jérôme Genest, Michel Piché, and Réal Vallée

Centre d'Optique, Photonique et Laser (COPL), Université Laval, Québec G1V 0A6, Canada
**Corresponding author: simon.duval.2@ulaval.ca*

Received 20 March 2015; revised 9 June 2015; accepted 9 June 2015 (Doc. ID 234676); published 2 July 2015

Ultrafast fiber lasers operating in the near-infrared have revolutionized laser science by enabling numerous breakthroughs in both fundamental science and industrial applications. In this Letter, we extend the spectral coverage of these laser sources to the mid-infrared by reporting the first femtosecond fiber laser operating near 3 μm. This passively mode-locked fiber ring laser based on nonlinear polarization evolution in an Er^{3+}-doped fluoride glass fiber generates 207 fs pulses at 2.8 μm with an estimated peak power of 3.5 kW. This demonstration paves the way for further developments of promising applications in the molecular fingerprint region such as frequency comb spectroscopy.

OCIS codes: (060.3510) Lasers, fiber; (140.4050) Mode-locked lasers; (140.3070) Infrared and far-infrared lasers; (060.2410) Fibers, erbium; (060.5530) Pulse propagation and temporal solitons.

http://dx.doi.org/10.1364/OPTICA.2.000623

Femtosecond fiber lasers emitting in the near-infrared (0.7–2 μm) have not only fueled the development of ultrafast laser science, but also enabled several promising applications for the broader scientific community. These simple, compact, and reliable sources are now in fact routinely used for laser micromachining, biomedical imaging, and spectroscopy [1]. However, the spectral coverage of ultrafast fiber lasers is currently limited by the use of silica fibers that are no longer transparent at wavelengths beyond 2 μm [2]. This fundamental issue has hindered the development of femtosecond fiber lasers in the mid-infrared (mid-IR) spectral range (2–20 μm), also referred to as the molecular fingerprint region [3]. By producing a stable and coherent emission of high-peak-power pulses covering a broad spectrum, mid-IR ultrafast fiber lasers have the potential to become ideal sources for ultrabroad and ultrasensitive molecular spectroscopy [4] through the generation of supercontinuum [5] and optical frequency combs [3]. Medical applications such as minimally invasive skin surgeries [6] or breath analysis [7] could also greatly benefit from these laser sources.

In recent years, the availability of high-purity fluoride glass fibers that transmit at up to 5 μm has enabled the development of fiber lasers operating at wavelengths well above the 2.2 μm multiphonon edge of silica [2]. These lasers have been mainly developed near 3 μm because of the efficient emission bands of Er^{3+} (2.75 μm) and Ho^{3+} (2.85 μm) cations in fluoride glass fibers that can be readily pumped by standard near-infrared laser diodes. For instance, an efficient continuous-wave fluoride glass fiber laser delivering average output powers up to 27 W was demonstrated at 2.8 μm [8].

Pulsed versions of 3 μm fiber lasers were also demonstrated in order to access higher peak powers. Active *Q*-switching based on acousto-optic modulators was implemented in linear cavities, producing pulses as short as 78 ns [9], with peak powers up to 0.9 kW [10]. Passive techniques were also reported based on various saturable absorbers leading to *Q*-switching with partial mode-locking operation with pulse durations now on the order of 20 ps [11,12]. However, the previous lasers were reported to be unstable with respect to mode-locking operation due to nonoptimal cavity configuration. This issue was addressed more recently by two groups. Haboucha *et al.* reported a stable mode locking from an Er^{3+}: fluoride glass fiber laser operating at 2.8 μm by using a semiconductor saturable absorber mirror in conjunction with a fiber Bragg grating (FBG) in a linear cavity configuration [13]. In this laser, the use of an FBG allowed for the generation of a stable, self-starting pulse train with a repetition rate of 51.75 MHz and an estimated pulse duration of 60 ps. In parallel, Hu *et al.* demonstrated the first stable mode-locked fiber ring laser near 2.9 μm using an InAs saturable absorber in transmission and a holmium–praseodymium codoped ZBLAN fiber [14]. This configuration enabled the generation of 6 ps pulses with a peak power of 465 W. This is, to the best of our knowledge, the shortest pulse ever produced directly from a fiber oscillator at a wavelength above 2.2 μm.

In this Letter, we present the first 3 μm class femtosecond fiber laser. This laser produces 207 fs soliton pulses at 2.8 μm with a repetition rate of 55.2 MHz. It is also the first demonstration of an Er^{3+}: fluoride fiber-based laser that generates stable mode-locked pulses with peak powers in the kilowatt range (P_{peak}~ 3.5 kW).

The schematic of the laser is shown in Fig. 1. This simple ring cavity contains 3 meters of double-clad Er^{3+}: fluoride fiber (Le Verre Fluoré). The fiber has a 7 mol.% Er^{3+}-doped core (NA = 0.12) with a diameter of 15 μm that is surrounded by a 260 μm diameter cladding. The circular symmetry of the cladding is broken by two parallel flats separated by 240 μm. A fluoroacrylate polymer of lower refractive index surrounds this cladding, enabling multimode propagation of the pump beam

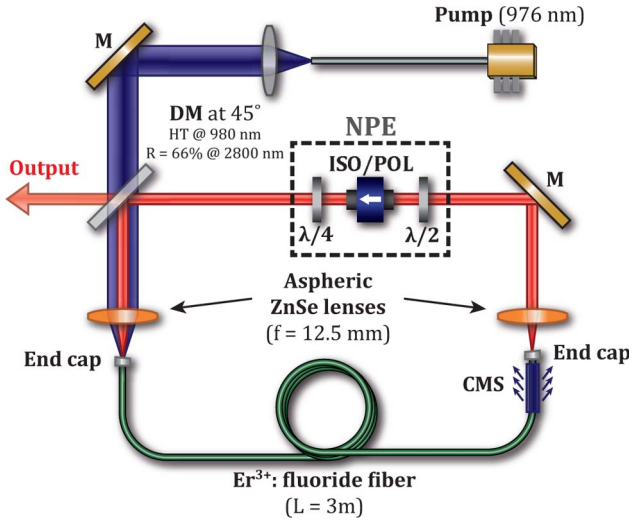

Fig. 1. Schematic of the laser cavity. DM, dichroic mirror; M, gold-coated mirrors; ISO/POL, optical isolator also used as a polarizer; $\lambda/4$, quarter waveplate; $\lambda/2$, half-waveplate; CMS, cladding mode stripper.

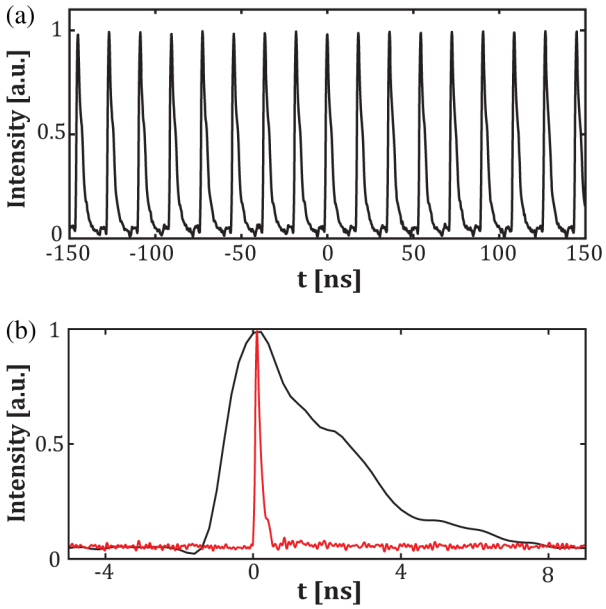

Fig. 2. (a) Measured output pulse train with a 2 ns rise time detector. The corresponding repetition rate is 55.2 MHz. (b) Zoom on one pulse of the 2.8 μm output (black) and the second harmonic (red) signal measured with a 100 ps rise time detector.

(NA > 0.46). The fiber dispersion ($\beta_2 = -0.086$ ps^2/m at 2.8 μm) was estimated based on both its material composition and guidance properties [15]. End caps made of a short segment (L ~ 700 μm) of multimode AlF_3 fiber (FiberLabs AMF-200/240) were spliced on both ends of the fiber to prevent fiber tip degradation. This degradation can arise either from OH diffusion and related thermal runaway [16] or from spurious laser spikes due to Q-switching instabilities. The end caps were angle-cleaved at 4° to avoid parasitic reflections that are detrimental for mode locking. The fiber is pumped with a multimode laser diode that delivers up to 7 W of continuous power at 976 nm. The pump signal is coupled inside the ring cavity through a homemade dichroic mirror that also serves as the output coupler for the 2.8 μm laser signal. This dichroic mirror has a transmission of >90% at 976 nm and a reflectivity of 66% at 2.8 μm, extracting 34% of the laser signal out of the cavity. Coupling of both laser and pump signals into the fiber is performed via aspheric ZnSe lenses ($f = 12.5$ mm). A cladding mode stripper (CMS in Fig. 1) made of a few centimeters of active fiber stripped and recoated with UV-curable, high-index polymer ($n = 1.54$) is fabricated at the end of the fiber segment in order to reject the residual pump power. Mode locking is initiated and maintained by nonlinear polarization evolution (NPE) [17] via the use of a quarter waveplate, half-waveplate, and optical isolator (Altechna). The isolator, based on Faraday rotation, also acts as a polarizer and ensures a unidirectional (counterclockwise in Fig. 1) propagation of the laser signal in the ring cavity. The total length of the free-space-propagation segment in the cavity is about 90 cm.

For a proper adjustment of the waveplates, the laser produces a stable, self-starting mode-locked pulse train. Mode-locked operation is maintained over several hours, with an rms fluctuation of the average output power of less than 1%. Also note that no noticeable degradation of the laser output performance was observed after several months of use. The temporal trace of the output signal is shown in Fig. 2(a), and was measured with a nitrogen-cooled HgCdTe photodiode connected to a preamplifier (Kolmar Technologies, rise time <2 ns). Since faster photodiodes are available at 1.5 μm, the second-harmonic (SH) signal was generated by focusing the output beam through a beta–barium borate crystal. The SH signal was then monitored with a photodetector (Alphalas, rise time <100 ps). As shown in Fig. 2(b), both 2.8 μm and SH signals show no evidence of multipulsing in the cavity. The repetition rate of the laser as measured with a radiofrequency spectrum analyzer is 55.2 MHz, in agreement with the effective cavity length of about 5.4 m.

To further confirm single-pulse operation and to measure the pulse temporal profile, the autocorrelation (AC) of the output signal was performed using a commercial autocorrelator covering wavelengths up to 3 μm (Femtochrome FR-103XL/IR/1700). The autocorrelation trace is shown in Fig. 3 along with the computed AC trace of an ideal $\text{sech}^2(t)$ temporal profile. The corresponding pulse full width at half-maximum (FWHM) is 207 fs. It is worth mentioning that the calibration factor of the autocorrelator was verified experimentally to ensure the validity of the measurement. No secondary peaks were observed over the total 200-ps scan range of the autocorrelator. The autocorrelation

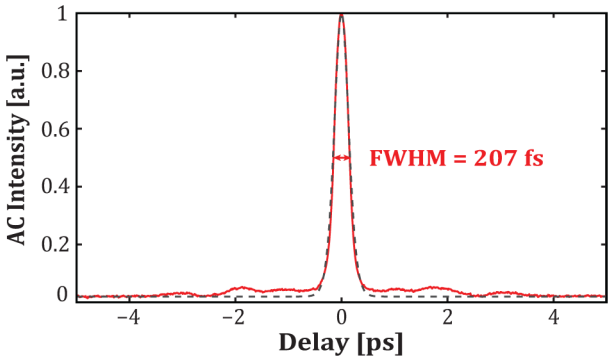

Fig. 3. Measured AC trace of the output beam (red) and the corresponding AC trace of a theoretical pulse with a $\text{sech}^2(t)$ shape and FWHM of 207 fs (dashed gray).

along with the measured pulse trains of both the mid-IR and SH signals confirm altogether that only one pulse is circulating in the cavity. The measured average output power is 44 mW, corresponding to a pulse energy of 0.8 nJ. Assuming a $\mathrm{sech}^2(t)$ temporal profile with a FWHM of 207 fs, the estimated pulse peak power is 3.5 kW.

The output spectrum presented in Fig. 4 (blue curve) was obtained using an optical spectrum analyzer (OSA) that covers wavelengths from 1.9 to 3.4 μm (Yokogawa, AQ6375L). The long free-space propagation (~2m) in the OSA greatly affects the spectrum of the signal due to environmental water vapor absorption near 2.8 μm. To quantify this impact, we monitored with the OSA the spectrum from a homemade flat mid-IR supercontinuum source and subtracted the environmental absorption background (black curve) from the signal. By doing so, the actual fiber laser spectrum impinging on the OSA could be inferred (red curve).

The output spectrum contains strong spectral peaks symmetrically located on both sides of the central wavelength $\lambda_c = 2805$ nm. These spectral features, referred to as Kelly sidebands, are clear evidence that the laser operates in the soliton regime [18]. From the temporal viewpoint, the Kelly sidebands correspond to resonant dispersive waves that copropagate with the soliton inside the cavity. The temporal modulations that are visible on either side of the central peak in the AC trace (Fig. 3) are likely associated with the cross-correlation of the main soliton pulse with these dispersive waves [19]. Mode locking in the soliton regime was expected because the dispersion of the fluoride fiber is highly anomalous at 2.8 μm, whereas no dispersion compensation was added to the laser cavity. Knowing the frequency associated with each sideband, the overall dispersion of the cavity and the average pulse width of the circulating pulse can be inferred using the following equation [18]:

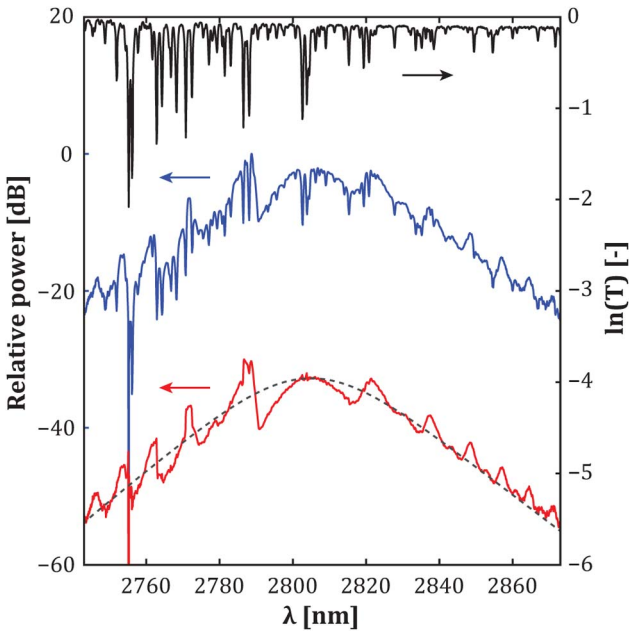

Fig. 4. Measured output spectrum (blue), natural logarithm of the atmospheric transmission for a 1 m propagation inside the OSA (black), reconstructed spectrum before the OSA (red), and theoretical spectrum of a $\mathrm{sech}^2(t)$ shape with FWHM of 230 fs (dashed gray).

$$(f_m - f_c)^2 = \frac{m}{\pi|B_2|} - \frac{1}{4\pi^2\tau^2}, \tag{1}$$

where m is the order of the sideband, f_m corresponds to the frequency of the sideband, $f_c = 1.07 \times 10^{14}$ Hz is the carrier frequency, B_2 is the overall cavity dispersion, and τ is the average pulse duration (FWHM ~1.763τ). By performing a linear regression of the frequency differences $(f_m - f_p)^2$ as a function of the integer m and using Eq. (1), we find an overall cavity dispersion $B_2 = -0.282$ ps^2. Assuming that the cavity dispersion is mostly governed by the dispersion of the 3 m segment of fluoride fiber, the fiber dispersion can be approximated by $\beta_2 = B_2/3\mathrm{m} = -0.094\mathrm{ps}^2/\mathrm{m}$, which is in good agreement with our previous estimation of $\beta_2 = -0.086$ ps^2/m.

The estimated average FWHM of the pulse in the cavity, also calculated from Eq. (1), is 328 fs. The production of output pulses (207 fs) shorter than the average soliton in the cavity is expected considering the relation between the energy of a soliton E_s and its duration τ [20]:

$$E_s = 2P_s\tau = \frac{2|\beta_2|}{\gamma\tau}, \tag{2}$$

where P_s is the peak power and γ and β_2 are respectively the nonlinear and the dispersion parameters of the fiber. This relation indicates that the soliton duration gets shorter as its energy increases. The circulating pulse therefore reaches maximum energy and thus shorter duration at the end of the gain fiber. Consequently, a pulse of minimum duration will be extracted out of the cavity at each roundtrip because the free space propagation through the NPE system can only further reduce its duration.

The best fit for the reconstructed output spectrum was obtained with the spectrum corresponding to an ideal soliton pulse with a $\mathrm{sech}^2(t)$ temporal profile and a FWHM of 230 fs (dashed gray curve). Both spectra are in good correspondence except near the center, where strong modulations are observed in the experimental spectrum. These modulations are actually resulting from the interference between the main pulse and the dispersive waves. Since the most intense sidebands are very close to the center of the spectrum because the overall dispersion of the cavity is high [see Eq. (1)], these modulations are more pronounced near its center. Since second-harmonic generation filters the low-intensity components of a signal, we measured the spectrum of the SH signal in order to get a better idea of the spectral properties of the output pulse without interference from dispersive waves. As shown in Fig. 5, the SH signal spectrum is consistent with the computed SH signal of an ideal 207 fs soliton pulse, which is in agreement with the temporal characteristics of the pulse inferred from the autocorrelation.

Interesting features stand out from these results. First, the intracavity water vapor absorption around 2.8 μm does not inhibit the formation of femtosecond pulses with a spectrum extending over more than 100 nm. This observation was also made in Cr^{2+}-based solid-state femtosecond lasers and can be turned into an advantage for intracavity spectroscopy with enhanced sensitivity [21]. Preliminary numerical simulations of the laser dynamics suggest that soliton shaping in the fiber segment compensates for this absorption, leading to a stable steady-state, mode-locked operation. Another important feature is that high-energy solitons (0.8 nJ) are generated from this fiber laser operated in the highly anomalous dispersion regime. This can be understood knowing that pulse shaping in the cavity strongly depends on the nonlinear

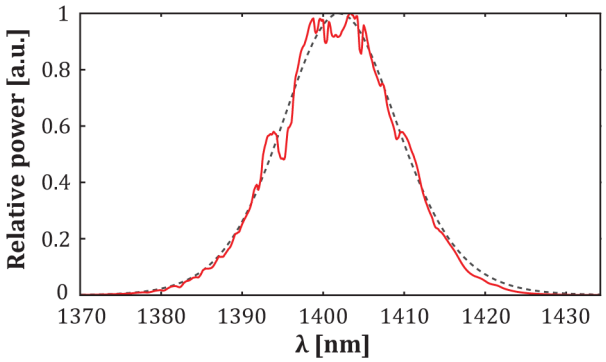

Fig. 5. Measured output spectrum of the SH signal (red) and the calculated SH signal of a theoretical pulse with a $\mathrm{sech}^2(t)$ shape and FWHM of 207 fs (dashed gray).

parameter γ, which scales as λ^{-3} [2,20]. Therefore, with the use of fluoride fibers that have dispersive and nonlinear properties similar to silica fibers, pulses of higher energy are expected for lasers emitting at longer wavelengths. We can thus expect to develop mid-IR fiber lasers with improved performance compared to those in the near-IR. Nevertheless, dispersion management in mid-IR fiber oscillators for the generation of shorter pulses remains the biggest challenge, as fluoride fibers possess a highly anomalous dispersion at these wavelengths.

Further performance improvements are expected in the near future with this fiber ring laser. Numerical modeling will offer good indications for determining the optimal fiber length and laser output coupling required in order to attain the highest peak power and shortest pulse duration. External amplification of these pulses with an Er^{3+}: fluoride fiber is also very promising for reaching the higher peak powers required for some applications such as supercontinuum generation [5]. Coherent spectral broadening of the laser output signal over more than one octave using, for example, a tapered chalcogenide fiber [22] combined with the recent demonstration of an active frequency reference operating near 3 μm [23] could provide the conditions to perform fully self-referenced frequency comb spectroscopy in the mid-infrared [3,24].

In summary, we have demonstrated the generation of stable soliton pulses from a passively mode-locked ring laser that includes a 3 m piece of Er^{3+}: fluoride fiber. The simple mode-locking system based on NPE in the fiber enables the production of 207 fs pulses with ~3.5 kW of peak power, surpassing all previous performances of mode-locked fiber lasers emitting around 3 μm. Dispersion of the fluoride fiber at 2.8 μm ($\beta_2 \sim -0.094$ ps^2/km) was also evaluated experimentally for the first time using the spectral positions of the Kelly sidebands. This demonstration clearly constitutes a major step toward the development of efficient femtosecond fiber sources operating in the mid-IR.

Funding. Canada Foundation for Innovation (Fondation canadienne pour l'innovation) (GF072345); Fonds de Recherche du Quebec Nature et Technologie (FRQ-NT) (FT097991); Natural Sciences and Engineering Research Council of Canada (Conseil de Recherches en Sciences Naturelles et en Génie du Canada) (CG101779).

Acknowledgment. The authors thank Adil Haboucha and Michel Olivier for helpful discussions, and Marc D'Auteuil and Souleymane Toubou Bah for the fabrication of the dichroic mirror at the COPL.

REFERENCES

1. M. E. Fermann and I. Hartl, Nat. Photonics **7**, 868 (2013).
2. S. D. Jackson, Nat. Photonics **6**, 423 (2012).
3. A. Schliesser, N. Picque, and T. W. Hansch, Nat. Photonics **6**, 440 (2012).
4. F. Tittel, D. Richter, and A. Fried, in *Solid-State Mid-Infrared Laser Sources*, I. Sorokina and K. Vodopyanov, eds., Vol. **89** of Topics in Applied Physics (Springer, 2003), pp. 458–529.
5. C. R. Petersen, U. Møller, I. Kubat, B. Zhou, S. Dupont, J. Ramsay, T. Benson, S. Sujecki, N. Abdel-Moneim, Z. Tang, D. Furniss, A. Seddon, and O. Bang, Nat. Photonics **8**, 830 (2014).
6. S. Amini-Nik, D. Kraemer, M. L. Cowan, K. Gunaratne, P. Nadesan, B. A. Alman, and R. J. D. Miller, PLoS One **5**, e13053 (2010).
7. C. Wang and P. Sahay, Sensors **9**, 8230 (2009).
8. V. Fortin, M. Bernier, N. Caron, D. Faucher, M. E. Amraoui, Y. Messaddeq, and R. Vallée, Opt. Eng. **52**, 054202 (2013).
9. T. Hu, D. D. Hudson, and S. D. Jackson, Opt. Lett. **37**, 2145 (2012).
10. S. Tokita, M. Murakami, S. Shimizu, M. Hashida, and S. Sakabe, Opt. Lett. **36**, 2812 (2011).
11. C. Wei, X. Zhu, R. A. Norwood, and N. Peyghambarian, Opt. Lett. **37**, 3849 (2012).
12. J. Li, D. D. Hudson, Y. Liu, and S. D. Jackson, Opt. Lett. **37**, 3747 (2012).
13. A. Haboucha, V. Fortin, M. Bernier, J. Genest, Y. Messaddeq, and R. Vallée, Opt. Lett. **39**, 3294 (2014).
14. T. Hu, D. D. Hudson, and S. D. Jackson, Opt. Lett. **39**, 2133 (2014).
15. L. Zhang, F. Gan, and P. Wang, Appl. Opt. **33**, 50 (1994).
16. N. Caron, M. Bernier, D. Faucher, and R. Vallée, Opt. Express **20**, 22188 (2012).
17. M. Hofer, M. Fermann, F. Haberl, M. Ober, and A. J. Schmidt, Opt. Lett. **16**, 502 (1991).
18. S. Kelly, Electron. Lett. **28**, 806 (1992).
19. K. Tamura, E. Ippen, and H. Haus, IEEE Photon. Technol. Lett. **6**, 1433 (1994).
20. G. P. Agrawal, *Nonlinear Fiber Optics*, 4th ed. (Academic, 2007).
21. I. Sorokina and E. Sorokin, IEEE J. Sel. Top. Quantum Electron. **21**, 273 (2015).
22. A. Marandi, C. W. Rudy, V. G. Plotnichenko, E. M. Dianov, K. L. Vodopyanov, and R. L. Byer, Opt. Express **20**, 24218 (2012).
23. M. Bernier, V. Michaud-Belleau, S. Levasseur, V. Fortin, J. Genest, and R. Vallée, Opt. Lett. **40**, 81 (2015).
24. I. Coddington, W. C. Swann, and N. R. Newbury, Phys. Rev. Lett. **100**, 013902 (2008).